# Contactless electroreflectance of Ga In N As Sb  Ga As single quantum wells with indium content of 8%–32%

R. Kudrawiec, H. B. Yuen, M. Motyka, M. Gladysiewicz, J. Misiewicz, S. R. Bank, H. P. Bae, M. A. Wistey, and James S. Harris

Citation: Journal of Applied Physics **101**, 013504 (2007); doi: 10.1063/1.2382721
View online: http://dx.doi.org/10.1063/1.2382721
View Table of Contents: http://scitation.aip.org/content/aip/journal/jap/101/1?ver=pdfcov
Published by the AIP Publishing

# Contactless electroreflectance of GaInNAsSb/GaAs single quantum wells with indium content of 8%–32%

R. Kudrawiec[a] and H. B. Yuen
*Solid State and Photonics Laboratory, Department of Electrical Engineering, 311X CISX, Via Ortega, Stanford University, Stanford, California 94305-4075*

M. Motyka, M. Gladysiewicz, and J. Misiewicz
*Institute of Physics, Wroclaw University of Technology, Wybrzeze Wyspianskiego 27, 50-370 Wrocław, Poland*

S. R. Bank, H. P. Bae, M. A. Wistey, and James S. Harris
*Solid State and Photonics Laboratory, Department of Electrical Engineering, 126X CISX, Via Ortega, Stanford University, Stanford, California 94305-4075*

(Received 1 May 2006; accepted 19 September 2006; published online 4 January 2007)

Interband transitions in GaInNAsSb/GaAs single quantum wells (SQWs) with nominally identical nitrogen and antimony concentrations (2.5% N and 7% Sb) and varying indium concentrations (from 8% to 32%) have been investigated by contactless electroreflectance (CER). CER features related to optical transitions between the ground and excited states have been clearly observed. Energies of the QW transitions extracted from CER measurements have been matched with those obtained from theoretical calculations performed within the effective mass approximation for various conduction-band offsets ($Q_C$) and various electron effective masses. It has been found that the $Q_C$ increases from 40% to 80% with the rise of the indium content from 8% to 32% and the electron effective mass is close to $0.09m_0$. The results show that the band gap discontinuity in GaInNAsSb/GaAs SQWs can be broadly tuned with a change in the indium concentration. © *2007 American Institute of Physics*. [DOI: 10.1063/1.2382721]

## I. INTRODUCTION

The GaInNAs alloy holds promise for the realization of high-performance laser diodes for telecommunications and solar-cell applications.[1–3] With concentrations of 6%–8% indium and 2%–3% nitrogen, GaInNAs has a band gap corresponding to 1.0 eV with little or no strain when grown upon GaAs. The ability to grow thick coherent layers ($\geqslant 1$ $\mu$m) is extremely important for high-quality absorption-based devices, such as solar cells and detectors. Before GaInNAs, GaAs-based devices requiring thick layers of 1.0 eV band gap material necessitated techniques such as graded strain relaxation layers or wafer bonding that introduced performance degrading defects. At higher concentrations of 30%–40% indium and 2%–3% nitrogen, GaInNAs has enabled GaAs-based long-wavelength edge-emitting and vertical-cavity surface-emitting lasers at 1.3 and 1.55 $\mu$m.[4–6] Before the development of GaInNAs, it was impossible to obtain these wavelengths from coherently grown material on GaAs due to the very high strain found within the active region. With nitrogen, although the strain is still very high ($\geqslant 2.0\%$), it is low enough that one to three quantum wells (QWs) may be grown. Most importantly, the emission from the QW shifts to the red at ~100 meV per 1% of nitrogen.

Antimony has been added as a surfactant and an incorporated group-V species during GaInNAs growth, improving the structural and optical quality of the material.[7–11] GaInNAsSb devices have shown remarkable progress towards the realization of low-cost telecommunication devices with the demonstration of the low-threshold 1.55 $\mu$m edge-emitting laser[12] and the electrically pumped 1.55 $\mu$m range vertical-cavity surface-emitting laser.[13] Antimony has also been utilized during GaInNAs growth for solar-cell material.

Despite strong progress in the development of devices, many fundamental material parameters, including the conduction-band offset ($Q_C$) and the electron effective mass ($m_e$), remain unknown or are not fully understood. Knowledge of these parameters is of great significance for a full exploration and optimization of this material system for device applications. The $Q_C$ for GaInNAs/GaAs QWs has been investigated many times.[14–20] There is general agreement that for GaInNAs/GaAs QWs with high indium content (In $>20\%$), the $Q_C$ does not vary significantly with a rise in nitrogen concentration and it can be assumed, in this case, that the $Q_C$ is close to 80%. Few investigations can be found for GaInNAs/GaAs QWs with low indium content due to decreased interest in these QWs. For indium concentrations below 20%, the $Q_C$ decreases to ~40%–50%.[15,16,21] For indium-free QWs (GaNAs/GaAs), a type-II discontinuity of the valence band had been suggested during early studies on this alloy.[22,23] However, recent investigations show that GaNAs/GaAs QWs are type-I structures with the $Q_C$ of 70%–90%.[24,25] The incorporation of antimony atoms into GaNAs/GaAs significantly changes the $Q_C$. In general, it has been observed that antimony atoms in III-V semiconductors lead to a decrease of $Q_C$. For $GaN_{0.02}As_{0.98-x}Sb_x$/GaAs QWs, it has been shown that the $Q_C$ decreases from 80% to

[a]Permanent address: Institute of Physics, Wroclaw University of Technology, Wybrzeze Wyspianskiego 27, 50-370 Wroclaw, Poland; electronic mails: robert.kudrawiec@pwr.wroc.pl and kudrawiec@snow.stanford.edu

 

50% when the antimony content increased from 0 to 11%.[26,27] For $Ga_{0.9}In_{0.1}N_{0.027}As_{0.973-x}Sb_x$/GaAs QWs with the antimony content changing from 0 to ~6%, the $Q_C$ decreases from 55% to 45%.[21] The incorporation of antimony atoms into GaInNAs/GaAs QWs can be used to tune the band gap discontinuities and improve the structural and optical quality. This phenomenon is important from the point of view of band gap engineering since it allows the control of the band gap discontinuity, the band gap energy, and the lattice strain more independently than in ternary or quaternary QWs (i.e., GaNAs/GaAs or GaInNAs/GaAs QWs).

Another important parameter used in band gap engineering and device design is the electron effective mass. The electron effective mass in dilute-nitride QWs has been predicted by theories[28–32] and observed experimentally[25,33–37] to be larger than those containing materials without nitrogen. In the case of GaNAs, there is an agreement that while the electron effective mass is increased with the presence of nitrogen, it was not as high as suggested by initial reports.[33] Few investigations dealing with the electron effective mass for GaInNAs(Sb) can be found.[15,16,18,21,38] It is generally accepted for GaInNAs(Sb) that the electron effective mass increases after the incorporation of nitrogen atoms as well. It is also expected that the absolute value of the GaInNAs(Sb) electron effective mass should be lower than GaNAs with the same nitrogen concentration according to a general trend in semiconductors described by the Kane model. This model shows that the electron effective mass is correlated with the band gap energy: a smaller band gap leads to a lower electron effective mass. The introduction of indium and antimony atoms into GaNAs decreases the electron effective mass in addition to decreasing the band gap energy. The absolute value of the electron effective mass in GaInNAsSb poses an open question.

In this paper, GaInNAsSb/GaAs single QWs (SQWs) with identical nitrogen content and antimony fluxes, and varying indium concentrations in the range of 8%–32%, are investigated by contactless electroreflectance (CER).[39–41] Similar to photoreflectance (PR), this technique is an excellent tool to investigate both the fundamental and higher order QW transitions due to its absorptionlike character and high sensitivity. However, this technique has a number of advantages over PR for the study of QW structures. CER does not require a laser as the pump beam and avoids the photoluminescence background due to this pump beam. Also, CER spectra are free of below-band-gap oscillation features, which are often observed in PR spectra, especially for GaAs-based structures grown on *n*-type GaAs substrates.[41] The analysis of CER data together with theoretical calculations makes it possible to determine material parameters such as the band gap discontinuity and the electron effective mass. Such procedures have been often applied in PR and CER studies for different semiconductor structures.[25–27,40,42,43] In this paper, the same approach has been applied to study the $Q_C$ and electron effective mass for GaInNAsSb/GaAs QWs with different indium contents.

## II. EXPERIMENTAL DETAILS

The GaInNAsSb/GaAs QW samples used in this study were grown on *n*-type (100) GaAs substrates by solid-source molecular beam epitaxy (MBE) in a Varian Mod Gen-II system. Gallium and indium were supplied by SUMO effusion cells. A valved arsenic cracker supplied $As_2$ and an unvalved antimony cracker supplied monomeric antimony. The GaInNAsSb QWs were grown at a substrate temperature of 440 °C measured by pyrometry. An arsenic-to-gallium overpressure of $2.0\times10^{-7}$ torr and an antimony flux of $1.0\times10^{-7}$ torr beam equivalent pressure were supplied during the GaInNAsSb QW growth. Nitrogen was supplied by a modified SVT Associates plasma cell operating at a rf of 13.56 MHz. Nitrogen gas of 5*N* (99.999%) purity was filtered through a <1 ppb (parts per $10^9$). Pall Mini-Gaskleen purifier to minimize oxygen contamination. The cell was operated with 300 W input power and a nitrogen gas flow of 0.5 SCCM (SCCM denotes cubic centimeter per minute at STP). Nitrogen incorporation into (In)GaAs is directly controlled by the group-III growth rate and obeys the equation

$$[\mathrm{N}\,\%] = \frac{K}{\{\mathrm{GR}\}}, \tag{1}$$

where [N%] is the percentage of nitrogen desired, $K$ is a constant obtained from calibrations, and {GR} is the group-III growth rate in $\mu$m/h.[44] The constant $K$ is a function of nitrogen gas flow[45] into the rf plasma cell and the amount of antimony[46–48] present in the dilute-nitride layer. The total group-III flux (gallium and indium) was held constant such that the nitrogen composition remained the same for all samples in this series. Different indium compositions were obtained by changing the ratio of indium and gallium fluxes. The structure for all samples consists of a 7.5 nm GaInNAsSb QW grown on a 300 nm GaAs buffer and capped by a 50 nm GaAs layer. The compositions of the samples were determined by high-resolution x-ray diffraction (HRXRD) and secondary-ion-mass spectrometry (SIMS).[49] HRXRD was obtained with a Philips X'Pert Pro four crystal high-resolution x-ray diffractometer and SIMS analysis from a Physical Electronics ADEPT 1010 quadrupole analyzer.

In order to measure CER spectra, a so-called "bright configuration" of the setup has been used.[50] Light from a halogen lamp (150 W) was reflected off the sample, sent through a single-grating 0.55 m focal length monochromator, and detected by an InGaAs *p-i-n* photodiode. Any significant differences between the classical "dark configuration" and the bright configuration were not observed within our experience.[51] Note that the illumination by white light can be treated as a constant modification of band bending in the investigated structure and it is not expected that this modification strongly affects energies of QW transitions for these samples. Samples for CER measurements were mounted in a capacitor. The top electrode of the capacitor is a copper-wire mesh and is semitransparent for light. This electrode was kept at a distance of 0.1–0.3 mm from the sample surface while the sample itself was fixed on the bottom copper electrode. A maximum peak-to-peak alternating voltage of ~1.9 kV was applied. The frequency of the ac voltage was

TABLE I. Room temperature binary material parameters used to calculate the strained quinary GaInNAsSb material parameters taken after Refs. 53 and 54.

| Parameter (unit) | GaN | GaAs | GaSb | InN | InAs | InSb |
|---|---|---|---|---|---|---|
| Heavy-hole mass $m_{hh}/m_0$ | 0.85 | 0.35 | 0.25 | 0.83 | 0.33 | 0.26 |
| Light-hole mass $m_{lh}/m_0$ | 0.24 | 0.09 | 0.044 | 0.16 | 0.027 | 0.015 |
| CB hydrostatic deformation potential $a^C$ (eV) | −6.71 | −7.17 | −7.5 | −2.65 | −5.08 | −6.94 |
| VB hydrostatic deformation potential $a^V$ (eV) | −0.69 | −1.16 | −0.8 | −0.7 | −1.0 | −0.36 |
| Shear deformation potential $b$ (eV) | −2.2 | −2.0 | −2.0 | −1.2 | −1.8 | −2.0 |
| Elastic constant $C_{11}$ (GPa) | 293 | 1221 | 884.2 | 187 | 832.9 | 684.7 |
| Elastic constant $C_{12}$ (GPa) | 159 | 566 | 402.6 | 125 | 452.6 | 373.5 |

285 Hz. Phase sensitive detection of the CER signal was made using a lock-in amplifier. Note that the PR technique, which is more common than CER, was not applied in this case because the QW samples were grown on *n*-type GaAs substrates. With these substrates, a below GaAs band gap oscillation is observed in PR spectra whereas such an oscillation is not observed in CER spectra.[41] In order to avoid the "oscillation issue" in this work, CER was applied rather than PR spectroscopy.

## III. THEORETICAL APPROACH

The calculations of QW energy levels have been performed within the framework of the effective mass approximation. The influence of strain on the band structure is taken into account, but excitonic effects are neglected. The biaxial strain was calculated based on the Pikus-Bir Hamiltonian.[52] For the $E_0$ critical point in GaInNAsSb ($\boldsymbol{k}=0$) the hydrostatic component of the strain, $\delta E_H$, shifts the valence and conduction bands. This total shift corresponds to the change in the band gap energy due to a hydrostatic deformation, which is proportional to the deformation potential $a$, that is measured. The total shift should be divided between the valence and conduction bands proportionally to the potential constants $a_V$ and $a_C$, where $a=a_V+a_C$. The shear component, $\delta E_S$, removes the valence-band degeneracy, giving a separate $E_{HH}$ (related to heavy holes) and $E_{LH}$ (related to light holes). For highly strained QWs, such as GaInNAsSb/GaAs QWs with high indium content, the strain-induced coupling with the spin-orbit split band cannot be neglected. Thus taking into account the coupling, the energies of the conduction and valence bands can be expressed in terms of the unstrained value as

$$E_C^{\ *} = E_C + \delta E_H^{\ C}, \tag{2a}$$

$$E_V^{\ HH} = E_V + \delta E_H^{\ V} + \delta E_S, \tag{2b}$$

$$E_V^{\ LH} = E_V + \delta E_H^{\ V} - \frac{1}{2}\left[\Delta - \delta E_S - \Delta\sqrt{1-2\frac{\delta E_S}{\Delta}+9\left(\frac{\delta E_S}{\Delta}\right)^2}\right], \tag{2c}$$

where $E_C$ and $E_V$ correspond to the energies of the conduction and valence bands at $\boldsymbol{k}=0$, respectively. The values of the $\delta E_H^{\ C}$, $\delta E_H^{\ V}$, and $\delta E_S$ are given by the following formulas:

$$\delta E_H^{\ C} = 2a^C\left(1-\frac{C_{12}}{C_{11}}\right)\varepsilon, \tag{3a}$$

$$\delta E_H^{\ V} = 2a^V\left(1-\frac{C_{12}}{C_{11}}\right)\varepsilon, \tag{3b}$$

$$\delta E_S = b\left(1-2\frac{C_{12}}{C_{11}}\right)\varepsilon, \tag{3c}$$

where $\varepsilon$ is the in-plane strain, $C_{11}$ and $C_{12}$ are elastic stiffness constants, and $b$ is the shear deformation potential. $\Delta$ is the energy between the valence and spin-orbit split bands and is 0.34 eV for GaAs. The value of $\Delta$ changes for GaInNAsSb and a linear interpolation between the $\Delta$ of the binary compounds does not work correctly (as is the case for the linear interpolation for the band gap energy). However, a linear interpolation for this parameter can be accepted as a first-order approximation, especially since an exact value of this parameter is not important for QWs with low indium content (samples with low strain since $\delta E_S/\Delta \ll 1$). Also for samples with high indium content, this parameter is not crucial in the calculations. Please note that this parameter influences energies of light-hole transitions only.

The material parameters necessary in the calculations conform with Vegard's law with good accuracy, contrary to the behavior mentioned for the band gap energy and the electron effective mass. Therefore, all the material parameters for $Ga_{1-x}In_xN_yAs_{1-y-z}Sb_z$ have been obtained by linear interpolation between the parameters of a relevant binary semiconductor[53,54] according to Eq. (4).

$$\begin{aligned} Q(x,y,z) = {} & (1-x)yQ_{GaN} + (1-x)(1-y-z)Q_{GaAs} \\ & + (1-x)zQ_{GaSb} + xyQ_{InN} + x(1-x-y)Q_{InAs} \\ & + xzQ_{InSb}, \end{aligned} \tag{4}$$

where $Q_i=b_i$ or $C12_i$ ($i$=GaN, GaAs, GaSb, InN, InAs, and InSb). The parameters of binary compounds used in the calculations are listed in Table I.

The conduction- and valence-band offsets, $Q_C$ and $Q_V$, are defined by Eq. (5) as

$$Q_C = \frac{\Delta E_C}{(\Delta E_C + \Delta E_V)} \times 100\,\%\,, \tag{5a}$$

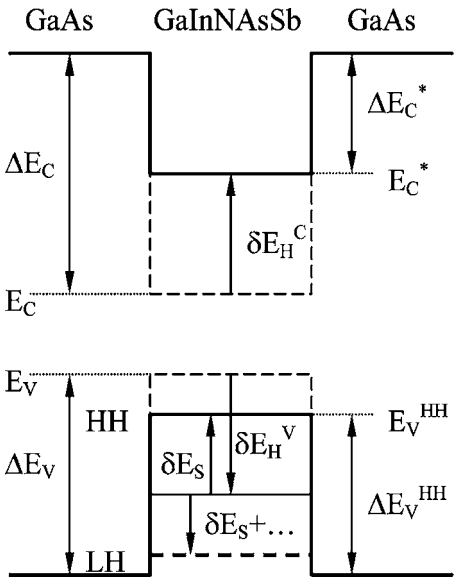


FIG. 1. Energy-band diagram in real space for compressively strained GaInNAsSb/GaAs QWs.

$$Q_V = (100\,\% - Q_C), \tag{5b}$$

where $\Delta E_C$ and $\Delta E_V$ are the conduction- and valence-band discontinuities at the heterojunction for unstrained materials, as illustrated in Fig. 1. They are designated *unstrained* because they are the "natural" band offset corresponding to the *ab initio* calculations[55] and the experimental values extracted from x-ray photoemission measurements. From a laser device perspective, the most interesting values are the band gap discontinuities with the strain corrections, shown in Fig. 1 as $\Delta E_C^*$ and $\Delta E_V^{HH}$. Generally, the most appropriate approach to heterojunction band offsets is to determine the $Q_C$ (or $Q_V$) since a GaInNAsSb/GaAs QW can be grown on both GaAs and InP substrates. For identical QWs grown on different substrates, the $Q_C$ does not vary, whereas the $\Delta E_C^*$ and $\Delta E_V^{HH}$ discontinuities vary due to different lattice strains. Moreover, the values of $\Delta E_C^*$ and $\Delta E_V^{HH}$ discontinuities can be calculated if the unstrained natural offset, $Q_C$, is known. Thus the $Q_C$ value is more universal. In this paper, both the $Q_C$ and $\Delta E_C^*$ and $\Delta E_V^{HH}$ discontinuities are determined.

In the calculations, the $Q_C$ and electron effective mass are treated as free parameters. The band gap energy of the GaInNAsSb layer has been adjusted to the experimental value of the QW ground state transition on the basis of a series of calculations with various $Q_C$ and $m_e$. It was observed that the energy of the ground state transition does not vary significantly with the change in the $Q_C$. In addition, the energy difference between the QW levels (the most important criterion for the electron effective mass determination) is insensitive to small changes in the band gap energy. For example, the change in the GaInNAsSb band gap energy from 800 to 790 meV, at $Q_C$=70% and $m_e$=0.09$m_0$, changes the energy difference between the first and the second electron levels by less than 1 meV. Thus the band gap energy can be easily adjusted in the calculations. An error associated with the GaInNAsSb band gap energy exists, but this error does not influence the conclusion concerning the $\Delta E_C^*$, $\Delta E_V^{HH}$, and $m_e$ because this error is compensated by errors

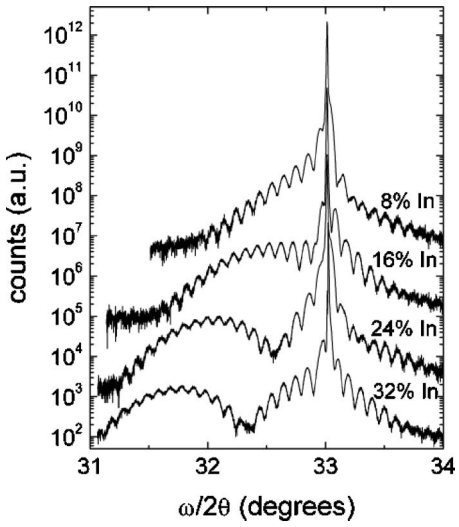


FIG. 2. (004) $\omega/2\theta$ HRXRD spectra of GaInNAsSb/GaAs QWs with varying indium concentrations.

associated with hydrostatic coefficients and elastic stiffness constants of the binary compounds. Note that with this approach, $\Delta E_C^*$, $\Delta E_V^{HH}$, and $m_e$ can be precisely determined despite the fact that a five element alloy is considered.

This situation is possible since, to solve the Schrödinger equation given by Eq. (6),

$$-\frac{\hbar^2}{2}\frac{\partial}{\partial z}\left[\frac{1}{m^*(z)}\frac{\partial f_n(z)}{\partial z}\right] + V(z)f_n(z) = E_n f_n(z), \tag{6a}$$

$$V(z) = \begin{cases} 0, & |z| < L_Z/2 \\ V_0, & |z| > L_Z/2, \end{cases} \tag{6b}$$

we only need to know three parameters: the QW depth ($V_0$), the effective mass in the (100) direction ($m^*$), and the QW width ($L_Z$). The $E_n$ and $f_n$ in Eq. (6a) are the energy and the wave function related to $n$ subband, respectively. $V_0$ corresponds to $\Delta E_C^*$, $\Delta E_V^{HH}$, and $\Delta E_V^{LH}$ for electrons, heavy holes, and light holes, respectively. $V_0$ is calculated by using several material parameters after Eqs. (2)–(4). The adjustment of the GaInNAsSb band gap energy to the ground state transition compensates errors from Eqs. (2)–(4), which are from inaccuracies of the material parameters for binary compounds. It should be noted that the $Q_C$ extracted from the analysis possesses a relative error higher than $\Delta E_C^*$, $\Delta E_V^{HH}$, and $m_e$.

## IV. RESULTS AND DISCUSSION

Figure 2 shows the HRXRD spectra obtained for the GaInNAsSb/GaAs QWs with different indium contents. All the samples have well defined QW signals and strong Pendellösung fringes, indicating good structural quality. As expected, a large change in strain is observed with the addition of indium. The strain increases from +0.7% at the low indium content to +2.0% in the high indium composition. In addition to HRXRD, SIMS has been employed to determine the composition of these samples.[49] A summary of the data is shown in Fig. 3. The indium, antimony, and nitrogen contents shown in Fig. 3 were used in the calculations. In this

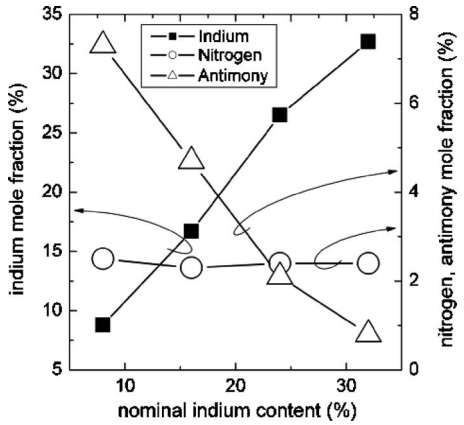


FIG. 3. Indium, nitrogen, and antimony compositions as a function of the intended indium content.

figure, it is seen that the indium content is very close to the intended value. The nitrogen composition for all four samples remains constant at 2.5%, whereas the antimony composition decreases with an increase of indium concentration. A detailed discussion on this issue can be found in Ref. 49.

The top panels in Figs. 4–7 show the room temperature CER spectra for GaInNAsSb/GaAs SQWs with 8%, 16%, 24%, and 32% In, respectively. All CER spectra are dominated by the GaAs band gap bulklike signal at an energy of ~1.42 eV. Below the GaAs signal, CER features associated with the optical transitions in GaInNAsSb/GaAs SQW are clearly observed. These features are analyzed using the low-field electromodulation Lorentzian line shape functional form[40]

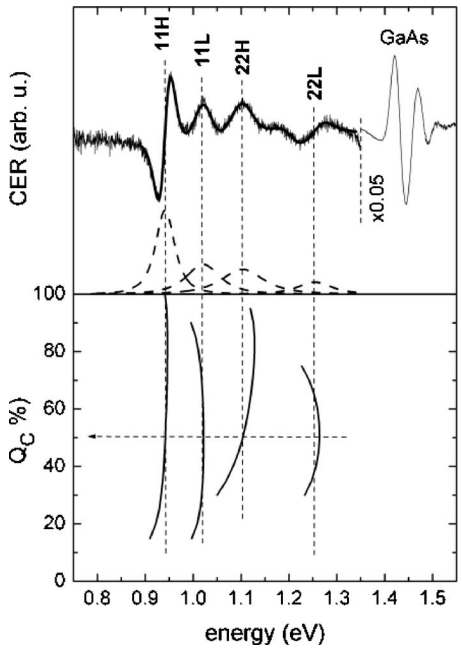


FIG. 5. Top panel: Room temperature CER spectra of the GaInNAsSb/GaAs SQW with 16% In content (solid line) together with the fitting curve (thick line) and the moduli of individual CER resonances (dashes lines). Bottom panel: Theoretical calculations performed for $m_e = 0.09m_0$ and various $Q_C$.

$$\frac{\Delta R}{R}(E) = \mathrm{Re}\left[\sum_{j=1}^{n} C_j e^{i\vartheta_j}(E - E_j + i\Gamma_j)^{-m_j}\right], \tag{7}$$

where $n$ is the number of the optical transitions and spectral functions used in the fitting procedure, $C_j$ and $\vartheta_j$ are the amplitude and phase of the line shape, and $E_j$ and $\Gamma_j$ are the

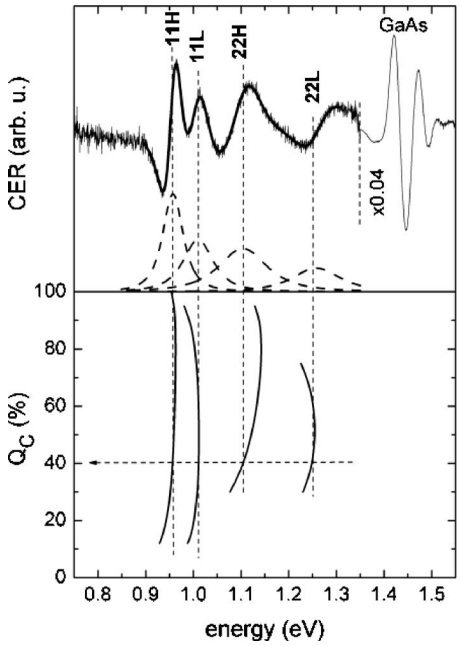


FIG. 4. Top panel: Room temperature CER spectra of the GaInNAsSb/GaAs SQW with 8% In content (solid line) together with the fitting curve (thick line) and the moduli of individual CER resonances (dashes lines). Bottom panel: Theoretical calculations performed for $m_e = 0.09m_0$ and various $Q_C$.

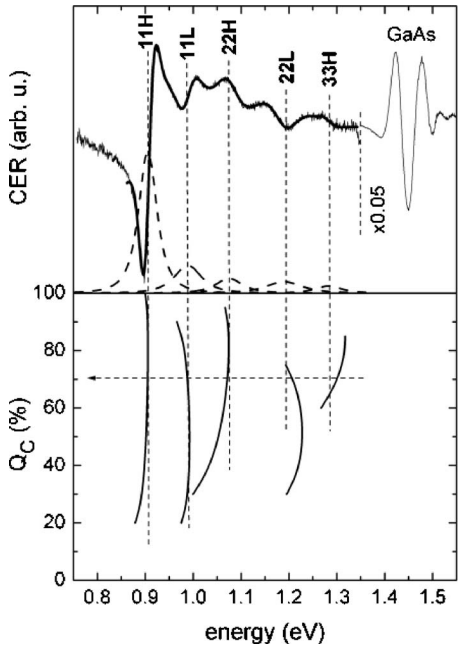


FIG. 6. Top panel: Room temperature CER spectra of the GaInNAsSb/GaAs SQW with 24% In content (solid line) together with the fitting curve (thick line) and the moduli of individual CER resonances (dashes lines). Bottom panel: Theoretical calculations performed for $m_e = 0.09m_0$ and various $Q_C$.

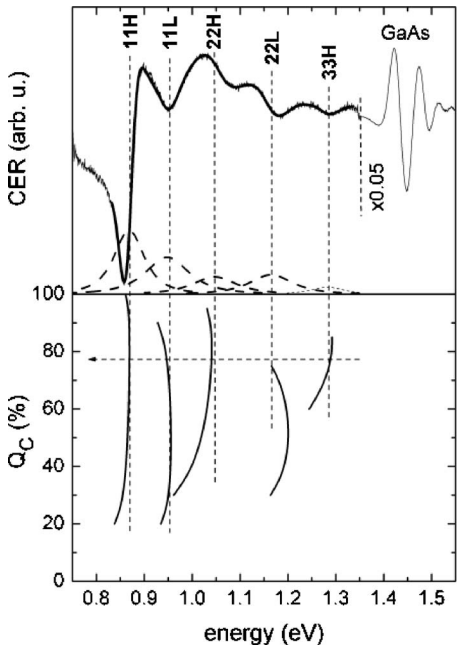


FIG. 7. Top panel: Room temperature CER spectra of the GaInNAsSb/GaAs SQW with 32% In content (solid line) together with the fitting curve (thick line) and the moduli of individual CER resonances (dashes lines). Bottom panel: Theoretical calculations performed for $m_e = 0.09m_0$ and various $Q_C$.

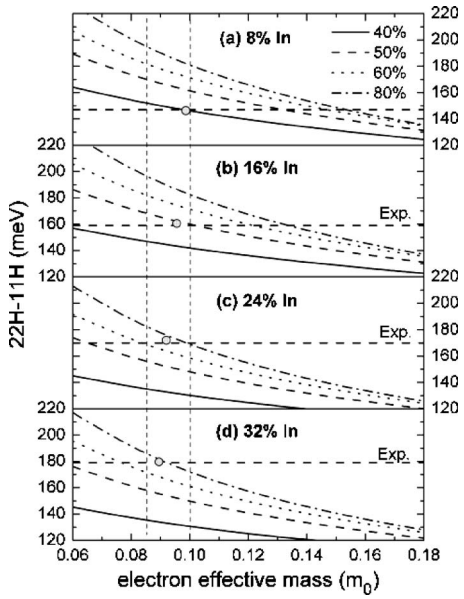


FIG. 8. Method used to analyze the $m_e$ in GaInNAsSb/GaAs SQWs with (a) 8% In, (b) 16% In, (c) 24%, In, and (d) 32% In. The horizontal dashed lines correspond to the energy difference between the 22H and 11H transitions taken from experimental data. The vertical thin dashed lines show the recommended range of the electron effective mass for these samples, whereas the dots mean the expected change in the electron effective mass.

energy and the broadening parameter of the transitions, respectively. The term $m$ refers to the type of optical transitions. In this case we assume that $m=3$. It corresponds to a one electron transition in a two dimensional system and is very close to the third derivative Gaussian line shape, i.e., the most appropriate line shape at room temperature. In Figs. 4–7 the fitting curves are shown as thick solid lines. In addition the moduli of individual resonances (dashed lines) obtained according to Eq. (8) are shown in these figures.

$$\Delta\rho_j(E) = \frac{|C_j|}{[(E-E_j)^2+\Gamma_j^2]^{m/2}}. \tag{8}$$

In general, the number of CER resonances necessary to simulate experimental data is decided by arbitrarily analyzing individual CER spectra by the naked eye (note that preliminary calculations help make a reasonable decision). It is obvious that a larger number of CER resonances better simulate experimental data but each resonance has to be justified since imaginary transitions can be generated if too many resonances were used to simulate a CER spectrum. Therefore, the moduli of individual CER resonances are plotted and evaluated. The evaluation means a comparison of transition intensities and the energy difference between individual resonances in order to eliminate resonances with strong overlap. Energies of CER resonances can be extracted from CER spectra with high accuracy (better than 1 meV) because of the differential character of CER lines and a lot of experimental points per one resonance (~200–300). However, for overlapping CER resonances the accuracy is worst. In our case, the energy error can be estimated by making fits with one or two resonances in different spectral regions. In order to simulate a signal originating from a neighbor resonance or a background signal, a linear or paraboliclike function can be added to Eq. (7). In this way, it has been estimated that the energy error for overlapping resonances is smaller than 5 meV. For CER resonances, which are well separated from neighbor resonances, the error has been estimated to be ~2 meV (see the moduli in Figs. 4–7 in order to compare the separation between CER resonances).

The identification of CER resonances was possible due to a series of calculations with various $Q_C$ and $m_e$. The notation $kl$H(L) denotes the transition between the $k$th heavy-hole (light-hole) valence subband and the $l$th conduction subband. The resonance at the lowest energy originates from the 11H transition, which is a fundamental transition for all SQW samples. In addition to the 11H transition, the CER spectra show an 11L transition (the lowest energy transition for light holes) and transitions between excited QW states such as 22H, 33H, and 22L. The partially forbidden transitions, such as the 31H transition, were also considered. However, it was concluded that they are weak in comparison with the allowed transitions and were neglected in the fitting procedure. In this manner, the number of CER resonances was reduced to the number of allowed transitions.

The bottom panels in Figs. 4–7 show the results of theoretical predictions for GaInNAsSb/GaAs SQWs considered in the figures. Such a plot allows us to attribute individual CER resonances to concrete QW transitions. In general, the results shown in the bottom part of Figs. 4–7 need many iterations with various $m_e$ (these iterations are not shown in the figures). Please note that in order to determine $Q_C$ and $m_e$, we carefully investigated the energy difference between QW transitions, making plots similar to those shown in Figs. 8 and 9 (these figures are discussed in the next part of the paper). Finally, Figs. 4–7 show the theoretical calculations

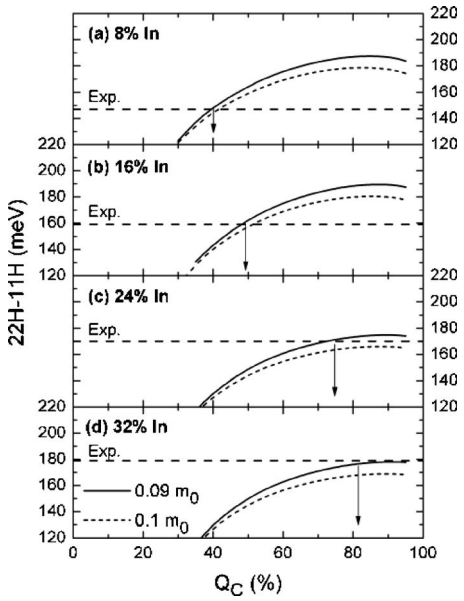


FIG. 9. Method used to analyze the $Q_C$ in GaInNAsSb/GaAs SQWs with (a) 8% In, (b) 16% In, (c) 24% In, and (d) 32% In. The horizontal dashed lines correspond to the energy difference between the 22H and 11H transitions taken from experimental data. The solid and dashed curves correspond to the energy difference between the 22H and 11H transitions obtained from the theoretical calculations with the electron effective mass of $0.1m_0$ and $0.09m_0$, respectively.

performed for the same electron effective ($m_e$=0.09$m_0$). Possible changes in the electron effective mass are discussed in the text.

For the GaInNAsSb/GaAs QW with 8% In content, four resonances have been resolved in the CER spectrum. The best agreement between experimental data and theoretical calculations was achieved for $Q_C$=40% and is consistent with previous investigations for GaInNAsSb/GaAs QWs with low indium content (8%) and with various antimony concentrations.[21] For increasing indium concentrations, the heavy-hole transitions evidently shift to the red, whereas the light-hole transitions do not shift. In addition, the splitting between the 11H and 11L transitions increases with an increase in indium content. The observed behavior of the light-hole transitions is typical for QWs with increasing compressive strain (in this case the rise of indium content increases the strain in QWs). In addition, a CER resonance related to the 33H transition appears for QWs with 24% In and 32% In and is the result of a third electron level. The confinement of the third electron level is related to two effects: (i) the In-induced decrease of the band gap energy for GaInNAsSb and (ii) the In-induced increase in the $Q_C$ for this system. The second effect is clearly visible in Fig. 9. The best agreement between experimental data and theoretical calculations for the four samples is observed at various $Q_C$ and it is seen that the $Q_C$ increases with the rise of indium content. For the QW with 32% In concentration, the $Q_C$ is close to 80% and is consistent with previous studies for high indium content GaInNAsSb/GaAs QWs.[56] It has been shown that the $Q_C$ in GaInNAsSb/GaAs QWs can be tuned with the variation in indium content. The observed increase in $Q_C$ with increasing indium content is in agreement with literature data for antimony-free GaInNAs QWs.[15,16] The antimony-related contribution to the change in $Q_C$ is only a second order effect since the change in indium content is much larger than the change in antimony content, as seen in Fig. 3. Finally, it is concluded that the $Q_C$ and the band gap energy can be controlled in GaInNAsSb/GaAs QWs more easily compared to antimony-free systems since an increase in the indium content leads to an increase in the $Q_C$ value, whereas an increase in the antimony content leads to a decrease of the $Q_C$ value.[21] This conclusion is important for the optimization of GaInNAsSb-based laser structures. Moreover, it shows that QWs composed of quinary compounds have some advantages in comparison with QWs composed of ternary compounds for which an independent control of the band gap discontinuity and the band gap energy is impossible.

The second free parameter in the calculations is the electron effective mass. The high value of the electron effective mass in GaInNAsSb is related to the incorporation of nitrogen atoms. In the GaInNAsSb samples, the nitrogen content does not vary. Therefore, it can be assumed that the nitrogen-related increase for the electron effective mass is the same for all samples. Any possible differences in the electron effective mass are small since they are related to changes in the indium and antimony concentrations. Based on data from literature,[53] it has been estimated that the differences in the electron effective mass for the nitrogen-free samples are ~13%. Therefore, for the samples investigated in this paper, it can be assumed that the electron effective mass decreases by less than ~13% with a rise in indium content from 8% to 32%. This assumption leads to a narrow window of acceptable $m_e$ for our samples. An agreement between experimental data and theoretical predictions should appear for each sample at the same value of the $m_e$. This value is easy to locate in Fig. 8. It is clearly visible that the electron effective mass should be close to $0.09m_0$ for each sample. It is also apparent that the high value of the electron effective mass ($m_e > 0.12m_0$) is not appropriate for GaInNAsSb. This conclusion is consistent with the literature, since it can be assumed that the upper limit for the electron effective mass in GaInNAsSb, with 2.5% N content, corresponds to the electron effective mass in $GaN_{0.025}As_{0.975}$ [$(0.1–0.12)m_0$ according to the band anticrossing model[57,58] and Refs. 25 and 34–36]. Incorporation of indium and antimony atoms leads to a decrease of the electron effective mass. The mass should be smaller than $0.1m_0$. If we assume that the QW with 8% In content has an electron effective mass of $0.1m_0$, then the 13% change in the electron effective mass leads to a shift of $\Delta m_e = 0.013m_0$. For the sample with 32% In content, the electron effective mass should be close to $0.087m_0$. The expected trend towards lower electron effective masses with increasing indium content can be seen in Fig. 8.

The calculations shown in Figs. 4–7 were performed with the same electron effective mass, $m_e$=0.09$m_0$. The change in $m_e$ affects the conclusions relating to the $Q_C$ value. If the assumed electron effective mass is too high, the resultant conduction-band offset is also too large (this behavior is illustrated in Fig. 9). In order to estimate an error associated with this effect, the calculations were repeated for different

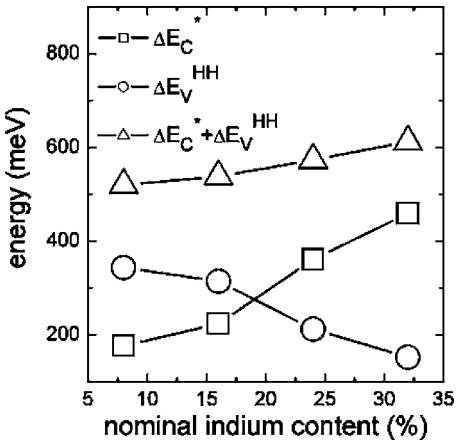


FIG. 10. Calculated variation of the $\Delta E_C^*$ and $\Delta E_V^{HH}$ discontinuities for GaInNAsSb/GaAs SQWs as a function of indium composition.

electron effective masses. Finally it has been concluded that the $Q_C$ in the samples is close to the value shown in Fig. 9 by the arrows.

Figure 10 shows the band gap discontinuities, $\Delta E_C^*$ and $\Delta E_V^{HH}$, obtained for the GaInNAsSb/GaAs QW samples. With an increase of indium concentration, the electron confinement depth increases while the depth of the heavy-hole confinement decreases. This phenomenon is related to the previously mentioned increase in the $Q_C$ due to an increase of the indium content. Also the observed change in antimony content influences the $\Delta E_C^*$ and $\Delta E_V^{HH}$. In a previous paper, it was shown that an increase of the antimony content in GaInNAsSb/GaAs QWs primarily increases the depth of the heavy-hole QW.[21] For the samples discussed in this paper, a decrease in antimony content appears with a rise of the indium content. However, the Sb-related contribution to changes in the band gap discontinuities is smaller than the In-related contribution since the absolute change in indium content is much larger than the change in antimony content.

## V. CONCLUSIONS

CER spectroscopy has been applied to investigate the interband transitions in GaInNAsSb/GaAs SQWs with various indium concentrations. The ground 11H and 11L transitions and the excited state transitions such as 22H, 22L, and 33H were clearly observed in the CER spectra. The experimental QW transition energies were compared with theoretical predictions based on an effective mass formalism model. The $Q_C$ and $m_e$ were varied to obtain a match between theory and measured data. It has been concluded that the $Q_C$ increases from 40% to 80% with an increase in indium content from 8% to 32%. It corresponds to an increase of the electron QW depth by a factor of ~2.5 (290 meV) and a decrease of the heavy-hole QW depth by a factor of ~2 (150 meV). These results demonstrate that the band gap discontinuity in GaInNAsSb/GaAs QW can be tuned by a change in indium composition. In addition, it has been shown that the electron effective mass for these QWs is close to $0.09m_0$.

## ACKNOWLEDGMENTS

The authors acknowledge the support from the Foundation for Polish Science through a Subsidy 8/2005, support under DARPA and ARO Contracts Nos. MDA972-00-1-024, DAAD17-02-C-0101, and DAAD199-02-1-0184, ONR Contract No. N00014-01-1-00100, as well as the Stanford Network Research Center (SNRC). One of the authors (R.K.) acknowledges support from the Foundation for Polish Science. Another author (H.B.Y.) acknowledges support from the Stanford Graduate Fellowships.

[1] M. Kondow, K. Uomi, A. Niwa, T. Kitatani, S. Watahiki, and Y. Yazawa, Jpn. J. Appl. Phys., Part 1 **35**, 1273 (1996).
[2] I. A. Buyanova, and W. M. Chen, *Physics and Applications of Dilute Nitrides* (Taylor & Francis, New York, 2004).
[3] M. Henini, *Dilute Nitride Semiconductors* (Elsevier, Oxford, 2005).
[4] K. D. Choquette *et al.*, Electron. Lett. **36**, 1388 (2000).
[5] N. Tansu and L. J. Mawst, IEEE Photonics Technol. Lett. **14**, 444 (2002).
[6] G. Jaschke, R. Averbeck, L. Geelhaar, and H. Riechert, J. Cryst. Growth **278**, 224 (2005).
[7] X. Yang, M. J. Jurkovic, J. B. Heroux, and W. I. Wang, Appl. Phys. Lett. **75**, 178 (1999).
[8] G. Ungaro, G. Le Roux, R. Teisser, and J. C. Harmand, Electron. Lett. **35**, 1246 (1999).
[9] H. Shimizu, K. Kumada, S. Uchiyama, and A. Kasukawa, Electron. Lett. **36**, 1379 (2000).
[10] X. Yang, J. B. Heroux, L. F. Mei, and W. I. Wang, Appl. Phys. Lett. **78**, 4068 (2001).
[11] V. Gambin, W. Ha, M. A. Wistey, H. B. Yuen, S. R. Bank, S. M. Kim, and J. S. Harris, IEEE J. Sel. Top. Quantum Electron. **8**, 795 (2002).
[12] S. R. Bank, H. P. Bae, H. B. Yuen, M. A. Wistey, L. L. Goddard, and J. S. Harris, Electron. Lett. **42**, 156 (2006).
[13] M. A. Wistey, S. R. Bank, H. P. Bae, H. B. Yuen, E. R. Pickett, L. L. Goddard, and J. S. Harris, Electron. Lett. **42**, 282 (2006).
[14] M. Hetterich, M. D. Dawson, A. Yu. Egorov, D. Bernklau, and H. Riechert, Appl. Phys. Lett. **76**, 1030 (2000).
[15] Z. Pan, L. H. Li, Y. W. Lin, B. O. Sun, D. S. Jiang, and W. K. Ge, Appl. Phys. Lett. **78**, 2217 (2001).
[16] J. B. Heroux, X. Yang, and W. I. Wang, J. Appl. Phys. **92**, 4361 (2002).
[17] S. A. Choulis, T. J. C. Hosea, S. Tomic, M. Kamal Saadi, A. R. Admas, E. P. O'Reilly, B. A. Weinstein, and P. J. Klar, Phys. Rev. B **66**, 165321 (2002).
[18] J. Misiewicz, R. Kudrawiec, K. Ryczko, G. Sęk, A. Forchel, J. C. Harmand, and M. Hammar, J. Phys.: Condens. Matter **16**, 3071 (2004).
[19] Gh. Dumitras and H. Riechert, J. Appl. Phys. **94**, 3955 (2003).
[20] M. Galluppi, L. Geelhaar, and H. Riechert, Appl. Phys. Lett. **86**, 131925 (2005).
[21] R. Kudrawiec *et al.*, Appl. Phys. Lett. **88**, 221113 (2006).
[22] S. Sakai, Y. Ueta, and Y. Terauchi, Jpn. J. Appl. Phys., Part 1 **32**, 4413 (1993).
[23] T. Kitani, M. Kondow, T. Kikawa, Y. Yazawa, M. Okai, and K. Uomi, Jpn. J. Appl. Phys., Part 1 **38**, 5003 (1999).
[24] S. Tomic, E. P. O'Reilly, P. J. Klar, H. Gruning, W. Heimbrodt, W. M. Chen, and I. A. Buyanova, Phys. Rev. B **69**, 245305 (2004).
[25] R. Kudrawiec, M. Motyka, M. Gladysiewicz, J. Misiewicz, J. A. Gupta, and G. C. Aers, Solid State Commun. **138**, 365 (2006).
[26] R. Kudrawiec, K. Ryczko, J. Misiewicz, H. B. Yuen, S. R. Bank, M. A. Wistey, H. P. Bae, and J. S. Harris, Jr., Appl. Phys. Lett. **86**, 141908 (2005).
[27] R. Kudrawiec, M. Gladysiewicz, J. Misiewicz, H. B. Yuen, S. R. Bank, M. A. Wistey, H. P. Bae, and J. S. Harris, Jr., Phys. Rev. B **73**, 245413 (2006).
[28] T. Mattila, S.-H. Wei, and A. Zunger, Phys. Rev. B **60**, R11245 (1999).
[29] C. Skierbiszewski *et al.*, Phys. Status Solidi B **216**, 135 (1999).
[30] A. Lindsay and E. P. O'Reilly, Solid State Commun. **112**, 443 (1999).
[31] I. Gorczyca, C. Skierbiszewski, T. Suski, N. E. Christensen, and A. Svane, Phys. Rev. B **66**, 081106 (2002).
[32] N. Shtinkov, P. Desjardins, and R. A. Masut, Phys. Rev. B **67**, 081202 (2003).
[33] Y. Zhang, A. Mascarenhas, H. P. Xin, and C. W. Tu, Phys. Rev. B **61**, 7479 (2000).

[34]C. Skierbiszewski *et al.*, Appl. Phys. Lett. **76**, 2409 (2000).
[35]P. N. Hai, W. M. Chen, I. A. Buyanova, H. P. Xin, and C. W. Tu, Appl. Phys. Lett. **77**, 1843 (2000).
[36]J. Wu, W. Shan, W. Walukiewicz, K. M. Yu, J. W. Ager III, E. E. Haller, H. P. Xin, and C. W. Tu, Phys. Rev. B **64**, 085320 (2001).
[37]C. Skierbiszewski, I. Gorczyca, S. P. Lepkowski, J. Lusakowski, J. Borysiuk, and J. Toivomem, Semicond. Sci. Technol. **19**, 1189 (2004).
[38]G. Baldassarri *et al.*, Phys. Rev. B **67**, 233304 (2003).
[39]X. Yin and F. H. Pollak, Appl. Phys. Lett. **59**, 2305 (1991).
[40]F. H. Pollak, in *Handbook on Semiconductors* edited by T. S. Moss (Elsevier Science, Amsterdam, 1994), Vol. 2, pp. 527–635.
[41]R. Kudrawiec, P. Sitarek, J. Misiewicz, S. R. Bank, H. B. Yuen, M. A. Wistey, and J. S. Harris, Jr., Appl. Phys. Lett. **86**, 091115 (2005).
[42]R. C. Tu *et al.*, J. Appl. Phys. **83**, 1043 (1998).
[43]M. Munoz, H. Lu, X. Zhou, M. C. Tamargo, and F. H. Pollak, Appl. Phys. Lett. **83**, 1995 (2003).
[44]S. G. Spruytte, M. C. Larson, W. Wampler, C. W. Coldren, H. E. Petersen, and J. S. Harris, Jr., J. Cryst. Growth **227–228**, 506 (2001).
[45]H. B. Yuen, M. A. Wistey, S. R. Bank, H. P. Bae, and J. S. Harris, Jr., J. Vac. Sci. Technol. B **23**, 1328 (2005).
[46]H. B. Yuen, S. R. Bank, M. A. Wistey, A. Moto, and J. S. Harris, Jr., J. Appl. Phys. **96**, 6375 (2004).
[47]H. B. Yuen, S. R. Bank, M. A. Wistey, J. S. Harris, Jr., M.-J. Seong, S. Yoon, R. Kudrawiec, and J. Misiewicz, J. Appl. Phys. **97**, 113510 (2005).
[48]K. Volz, V. Gambin, W. Ha, M. A. Wistey, H. B. Yuen, S. R. Bank, and J. S. Harris, Jr., J. Cryst. Growth **251**, 360 (2003).
[49]H. B. Yuen, S. R. Bank, H. P. Bae, M. A. Wistey, and J. S. Harris, J. Appl. Phys. **99**, 093504 (2006).
[50]R. Kudrawiec and J. Misiewicz, *E-MRS 2005 Spring Meeting, Strasbourg, France* [Appl. Surf. Sci. **253**, 152 (2006)].
[51]R. Kudrawiec (unpublished).
[52]G. L. Bir and G. Pikus, *Symmetry and Strain-Induced Effects in Semiconductors* (Wiley, New York, 1974).
[53]I. Vurgaftman, J. R. Meyer, and L. R. Ram-Mohan, J. Appl. Phys. **89**, 5815 (2001).
[54]I. Vurgaftman and J. R. Meyer, J. Appl. Phys. **94**, 3675 (2003).
[55]S.-H. Wei and A. Zunger, Appl. Phys. Lett. **72**, 2011 (1998).
[56]R. Kudrawiec, M. Gladysiewicz, J. Misiewicz, H. B. Yuen, S. R. Bank, M. A. Wistey, H. P. Bae, and J. S. Harris, Jr., Solid State Commun. **137**, 138 (2006).
[57]W. Shan, W. Walukiewicz, J. W. Ager III, E. E. Haller, J. F. Geisz, D. J. Friedman, J. M. Olson, and S. R. Krutz, Phys. Rev. Lett. **82**, 1221 (1999).
[58]W. Shan *et al.*, Phys. Status Solidi B **223**, 75 (2001).